RSC Advances

PAPER

View Article Online
View Journal | View Issue

Check for updates

Cite this: *RSC Adv.*, 2021, **11**, 10524

Ancillary ligand modulated stereoselective self-assembly of triple-stranded Eu(III) helicate featuring circularly polarized luminescence†

Zhiwei Yao, Yanyan Zhou, Ting Gao, Pengfei Yan* and Hongfeng Li*

Received 27th February 2021
Accepted 4th March 2021

DOI: 10.1039/d1ra01583d

rsc.li/rsc-advances

Creating optically pure metal assemblies is a hot research topic in the realms of chiral supramolecules. Here, three new triple-stranded europium(III) helicates $Eu_2L_3(L')_2$ [L = 4,4′-bis(4,4,4-trifluoro-1,3-dioxobutyl) diphenyl sulphide; L′ = 1,10-phenanthroline (Phen) or *R*/*S*-2,2′-bis(diphenylphosphinyl)-1,1′-binaphthyl (*R*/*S*-BINAPO)] were synthesized in order to investigate the effects of ancillary ligands on controlling the stereoselective self-assembly of lanthanide helicates. X-ray single crystal structure analysis showed that $Eu_2L_3(Phen)_2$ crystalized in an achiral space group $P\bar{1}$ with the equivalent amount of P and M helicates in one single cell. The isolated Eu_2L_3(*S*-BINAPO)$_2$ and Eu_2L_3(*R*-BINAPO)$_2$ were verified to be enantiopure by ^{1}H, ^{19}F, ^{31}P NMR and DOSY NMR analyses. Additionally, the mirror-image CD spectra also demonstrated the successful syntheses of the enantiomers and the presence of an effective chirality transformation from BINAPO to achiral L. Furthermore, the perfect mirror-image circularly polarized luminescence (CPL) spectra of Eu_2L_3(*S*-BINAPO)$_2$ and Eu_2L_3(*R*-BINAPO)$_2$ indicated the existence of the excited state chirality of the Eu^{3+} center associated with $|g_{lum}|$ values reaching 0.112. In addition, the photophysical properties of three helicates were also discussed.

Introduction

In recent years, circularly polarized luminescence (CPL) materials[1] have attracted great interest because of their potential application in 3D displays,[2] optical storage,[3] communication of spin information[4] and CPL probes.[5] Lanthanide helicates are regarded as the favorable candidates of CPL materials in view of their supramolecular helical chirality and the characteristic electron transition from Ln^{3+} ions.[6] The partial magnetic dipole character endowed the Ln^{3+} ions with a higher luminescence dissymmetry factor (g_{lum}),[7] typically in the range of 10^{-2}–0.5,[8] which is obviously larger than those of pure organic luminophores ($g_{lum} = 10^{-5}$–10^{-3}).[9] To date, the highest g_{lum} value for CPL materials in solution was recorded to be 1.38 from a Eu^{3+} complex, Cs[Eu((+)-hfbc)$_4$].[10]

On the other hand, the chirality amplification effect arising from the supramolecular chirality provides a structural foundation for the helicates to produce the large g_{lum} values. In 2009, Gunnlaugsson *et al.* prepared a chiral lanthanide helicate and reported its CPL property for the first time.[11] In recent years, Gunnlaugsson,[12] Sun,[13] and Law[14] have successfully prepared a few optical pure dinuclear lanthanide helicates based on chiral 2,6-dipicolinic amides derivatives, and some of which have been used for CPL study. Although the g_{lum} values were satisfactory, the examples for the preparation of chiral lanthanide helicates were still rare. The introduction of chiral ancillary ligand was proved to be an effective way to control the stereoselective of lanthanide assemblies.[15]

Our group has been concerned with the research of luminescent lanthanide helicates composed of β-diketonate ligands.[16] The highly effective sensitizing ability of β-diketones ensured the high luminescence quantum yields (QYs) of helicates. More recently, we reported several examples of chiral helicates featured with CPL properties, which showed the moderate $|g_{lum}|$ values.[17] Generally, the large degree of twisting of helix is favorable for chirality amplification, and probably brings the increase of luminescence dissymmetry.

Herein, three optical active and inactive helicates were constructed by employing an achiral Phen and two chiral *R*- and *S*-BINAPO as the second ligands. Single crystal X-ray crystallographic analysis showed $Eu_2L_3(Phen)_2$ was a racemic mixture with a pair of ΔΔ- and ΛΛ-helicate existing in one single cell. While the diastereoselective self-assembly during the preparation of Eu_2L_3(*S*-BINAPO)$_2$ and Eu_2L_3(*R*-BINAPO)$_2$ can be verified by NMR spectra and semiempirical geometry optimization. The photophysical measurements showed that the helicates all present the satisfactory luminescence quantum yields, 31% and 34% for $Eu_2L_3(Phen)_2$ and Eu_2L_3(*R*/*S*-BINAPO)$_2$, respectively. In addition, the chiral helicates Eu_2L_3(*S*-BINAPO)$_2$ and Eu_2L_3(*R*-

Key Laboratory of Functional Inorganic Material Chemistry, Ministry of Education, P. R. China, School of Chemistry and Materials Science, Heilongjiang University, Harbin 150080, P. R. China. E-mail: lihongfeng@hlju.edu.cn; yanpf@vip.sina.com

† Electronic supplementary information (ESI) available. CCDC 994501. For ESI and crystallographic data in CIF or other electronic format see DOI: 10.1039/d1ra01583d

Open Access Article. Published on 10 March 2021. Downloaded on 2/14/2026 12:17:19 PM.
This article is licensed under a Creative Commons Attribution-NonCommercial 3.0 Unported Licence.

© 2021 The Author(s). Published by the Royal Society of Chemistry

Open Access Article. Published on 10 March 2021. Downloaded on 2/14/2026 12:17:19 PM.
This article is licensed under a Creative Commons Attribution-NonCommercial 3.0 Unported Licence.

BINAPO)$_2$ present a modest circularly polarized luminescence dissymmetry ($|g_{lum}| = 0.112$ at 595 nm).

Results and discussion

Characterization of L and complexes

The syntheses routes of **L** and its corresponding complexes $Eu_2\mathbf{L}_3(Phen)_2$ and $Eu_2\mathbf{L}_3(R/S\text{-BINAPO})_2$ are outlined in Scheme 1. The C_2-symmetric achiral bis-β-diketone 4,4′-bis(4,4,4-trifluoro-1,3-dioxobutyl)phenyl sulphide (**L**) was prepared *via* two steps, the first was the Friedel–Crafts acylation of phenyl sulfide, then followed with a Claisen condensation of 4,4′-diacetyl phenyl sulfide and ethyl trifluoroacetate. The corresponding intermediate and ligand were characterized by ESI-TOF-MS and ^{1}H NMR (Fig. S1–S3†).

The triple-stranded helicates $Ln_2\mathbf{L}_3(\mathbf{L}')_2$ were isolated by stirring a 3 : 2 : 2 mixture of **L**, **L**′ and $LnCl_3\cdot 6H_2O$ (Ln = Gd, Eu) at room temperature in CH_3OH. High-resolution ESI-TOF-MS analyses affirmed the successful preparation of triple-stranded helicates. For instance, Fig. 1a presents three clusters of peaks, corresponding to the positive charged $[M + H]^+$, $[M + K]^+$ and $[M + Na]^+$ species of $Eu_2\mathbf{L}_3(S\text{-BINAPO})_2$, at *m*/*z* 2995.1158, 3017.1653 and 3033.1340. The mass spectra of the other complexes also showed the expected molecule ions peaks (Fig. S4–S7†). The assignments were further affirmed by comparing the isotopic distributions of the experimental with simulated results.

^{1}H, ^{31}P, ^{19}F NMR, and DOSY NMR results also supported the successful preparation of $Eu_2\mathbf{L}_3(S\text{-BINAPO})_2$ and $Eu_2\mathbf{L}_3(R\text{-BINAPO})_2$ and their stabilities in THF (Fig. 1b, S8 and S9†). As shown in Fig. 1b, ^{1}H NMR of $Eu_2\mathbf{L}_3(S\text{-BINAPO})_2$ shows a single set of clear and broadening signals from **L** and *R*/*S*-BINAPO. Considering the absence of C_3 symmetry of the helicates, three sets of H signals from three different ligands should be observed. However, with the influence of paramagnetism of Eu^{3+} ion, for instance, only a single peak attributed to methine H_C resonance of β-diketone was observed at 5.34 ppm, not the expected three peaks. A more facile way to infer the formation of a single species was the employment of ^{31}P and ^{19}F NMR, in which only the singlet peaks were observed (Fig. S8 and S9†). Additionally, one single diffusion rate of $Eu_2\mathbf{L}_3(S\text{-BINAPO})_2$ ($D = 5.88 \times 10^{-6}$ cm^2 s^{-1}) in ^{1}H NMR diffusion ordered spectroscopy (DOSY) also supported the presence a single species in THF (Fig. 1c).

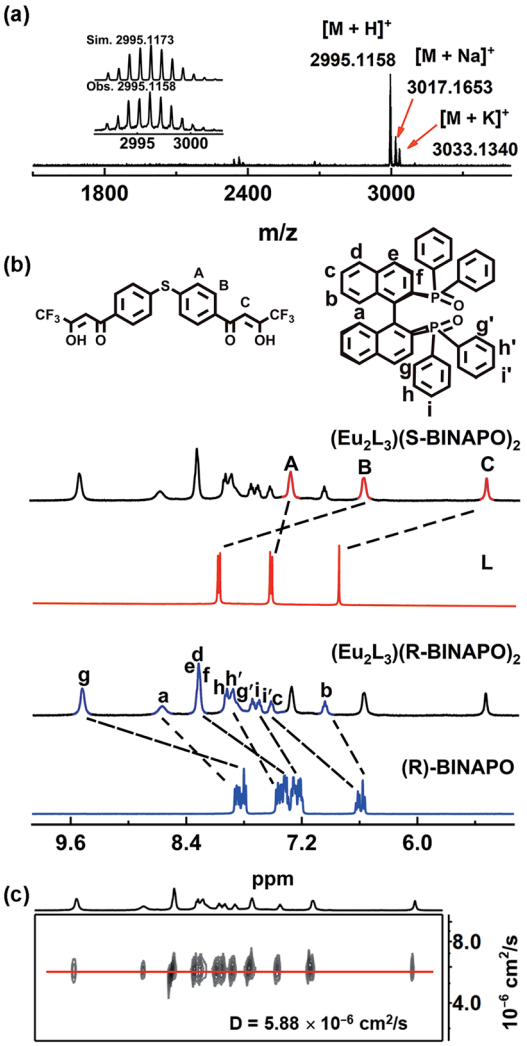

Fig. 1 (a) ESI-TOF-MS of $Eu_2\mathbf{L}_3(S\text{-BINAPO})_2$ with inset representing the simulated (Sim.) and observed (Obs.) isotopic distributions. (b) ^{1}H NMR (400 MHz) spectra of **L**, *R*-BINAPO and $Eu_2\mathbf{L}_3(R\text{-BINAPO})_2$ and $Eu_2\mathbf{L}_3(S\text{-BINAPO})_2$ (THF-d_8). (c) ^{1}H DOSY spectrum of $Eu_2\mathbf{L}_3(S\text{-BINAPO})_2$ in THF-d_8.

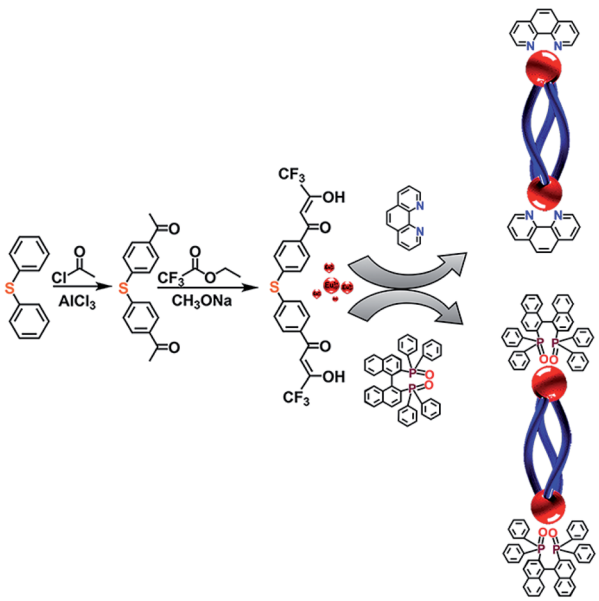

Scheme 1 Synthetic routes of **L** and the corresponding complexes $Eu_2\mathbf{L}_3(Phen)_2$ and $Eu_2\mathbf{L}_3(BINAPO)_2$.

X-ray single crystal structure of $Eu_2\mathbf{L}_3(Phen)_2$

The single crystals of $Eu_2\mathbf{L}_3(Phen)_2$ were grown by diffusion of diethyl ether to a THF/toluene solution of the complex. The structural analysis revealed that $Eu_2\mathbf{L}_3(Phen)_2$ was the expected triple-stranded helicate with each Eu^{3+} center ligated by six

Open Access Article. Published on 10 March 2021. Downloaded on 2/14/2026 12:17:19 PM.
This article is licensed under a Creative Commons Attribution-NonCommercial 3.0 Unported Licence.

oxygen (O) atoms from three β-diketones and two nitrogen (N) atoms from Phen (Fig. 2a), and adopting a square antiprism as coordination geometry (Fig. S10†). The Eu–N and Eu–O distances are in ranges of 2.331–2.383 Å and 2.574–2.617 Å, respectively. The Eu–Eu distance in one helicate reached to 13.229 Å. The corresponding crystallographic parameters were list in Table S1.† It was found that the $Eu_2\mathbf{L}_3(Phen)_2$ crystalized in an achiral triclinic space group $P\bar{1}$, where a pair of racemic mixtures of ΔΔ-$Eu_2\mathbf{L}_3(Phen)_2$ and ΛΛ-$Eu_2\mathbf{L}_3(Phen)_2$ were observed in one single cell. This result indicated that the absence of chiral element in self-assembly process will result in the formation of the racemic helicate.

As reported by us and others,[18] the chiral ancillary ligands could induce the metal supramolecule assemblies to form a single diastereoisomer. Herein, we employed the chiral BINAPO as ancillary ligands to construct the diastereopure helicates. Unfortunately, the single crystals of $Eu_2\mathbf{L}_3$(*R*/*S*-BINAPO)$_2$ were not obtained, although several methods had been tried. To better understand the chiral induction, we resorted to a molecular mechanical modeling built from LUMPAC 3.0 software with a Sparkle/RM1 model.[19] Taking the ΔΔ-$Eu_2\mathbf{L}_3$ helicate as an example, its assembly with *R*-BINAPO and *S*-BINAPO were both considered. As can be seen in Fig. S11,† the ΔΔ-$Eu_2\mathbf{L}_3$ with *R*-BINAPO as ancillary ligand has a relative lower system energy than that with *S*-BINAPO. Thus, it was proposed that the *R*-BINAPO could induce the $Eu_2\mathbf{L}_3$ to form P helical conformation with the metal center the ΔΔ configuration.

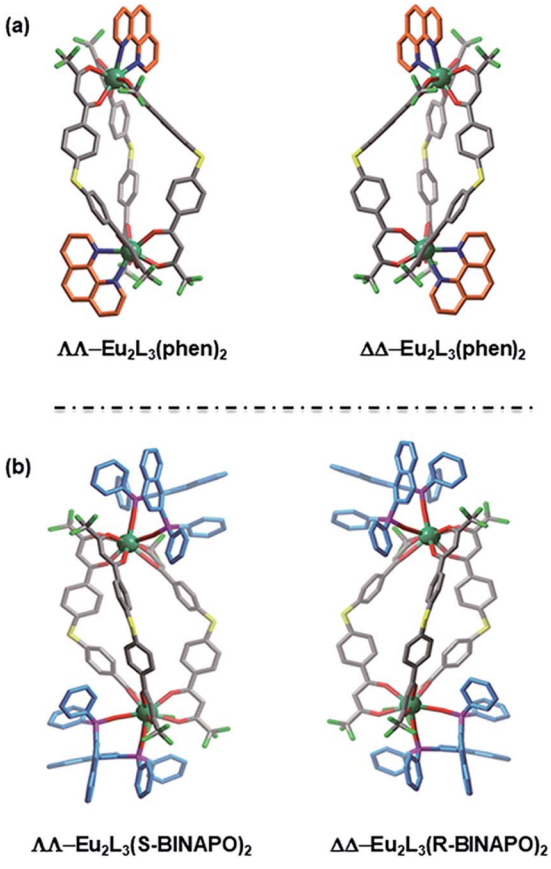

Fig. 2 (a) X-ray crystallographic structure of $Eu_2\mathbf{L}_3(Phen)_2$ and (b) Sparkle/RM1 optimized geometries of $Eu_2\mathbf{L}_3$(*S*-BINAPO)$_2$ and $Eu_2\mathbf{L}_3$(*R*-BINAPO)$_2$.

Photoluminescent properties of the complexes

The UV-vis spectra of $Eu_2\mathbf{L}_3(Phen)_2$, $Eu_2\mathbf{L}_3$(*R*/*S*-BINAPO)$_2$ and free **L** in THF are shown in Fig. 3. In free ligand, two clear bands with λ_{max} = 241 nm (1.8×10^4 dm^3 mol^{-1} cm^{-1}) and λ_{max} = 366 nm (4.1×10^4 dm^3 mol^{-1} cm^{-1}) were observed, which could be attributed to the π–π* transitions localizing at benzene ring and the ILCT transition from benzene ring to β-diketone units, respectively. In comparison with free ligand, three complexes all present the obvious hypsochromic shifts with the absorption maxima from 370 nm to 350 nm. This significant shift arose from the large twisting of **L** in complexes, which disrupted the conjugation of β-diketone moieties. While the high energy absorbances at 277 and 237 nm were attributed to the absorptions of Phen and *R*/*S*-BINAPO, respectively.

The excitation and emission spectra of three Eu^{3+} complexes are shown in Fig. 4 and S12.† Upon excitation at 370 nm, three Eu^{3+} complexes displayed five sharp emission bands at 580, 594, 613, 650 and 702 nm, respectively, relating to the $^5D_0 \rightarrow {}^7F_J$ (J = 0–4) transitions. In excitation spectra, the spectral bands could be well matched with the absorption bands of complexes in 280–400 nm regions, while the possible energy transfer from ancillary ligands could be excluded due to the absence of corresponding absorbance at high energy bands of 240–260 nm.

In emission spectra of Eu^{3+} complexes, the $^5D_0 \rightarrow {}^7F_2$ and $^5D_0 \rightarrow {}^7F_1$ transitions are of special importance. The former is the electric dipole hypersensitive transition, which is usually suggested to be sensitive to the coordination geometry of Eu^{3+} ion. Whereas, the $^5D_0 \rightarrow {}^7F_1$ transition is insensitive to the coordination sphere. Thus, the integrated intensity ratio of $I(^5D_0 \rightarrow {}^7F_2)/I(^5D_0 \rightarrow {}^7F_1)$ was often employed as a probe to infer the coordination geometry symmetry of Eu^{3+} ion, the larger of this value generally means the larger deviation of the Eu^{3+} from the highly symmetric coordination geometry.[20] Here, the intensity ratios reached to 25.4 and 28.3 for $Eu_2\mathbf{L}_3(Phen)_2$ and $Eu_2\mathbf{L}_3$(*R*/*S*-BINAPO)$_2$, respectively. It indicated the presence of a lower symmetry around Eu^{3+} ion.

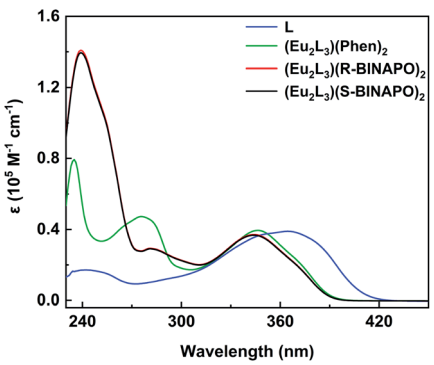

Fig. 3 UV-vis absorption spectra of **L** (3.3×10^{-6} M) and helicates $Eu_2\mathbf{L}_3(Phen)_2$ and $Eu_2\mathbf{L}_3$(*R*/*S*-BINAPO)$_2$ (1.0×10^{-5} M) in THF.

© 2021 The Author(s). Published by the Royal Society of Chemistry

Open Access Article. Published on 10 March 2021. Downloaded on 2/14/2026 12:17:19 PM.
This article is licensed under a Creative Commons Attribution-NonCommercial 3.0 Unported Licence.

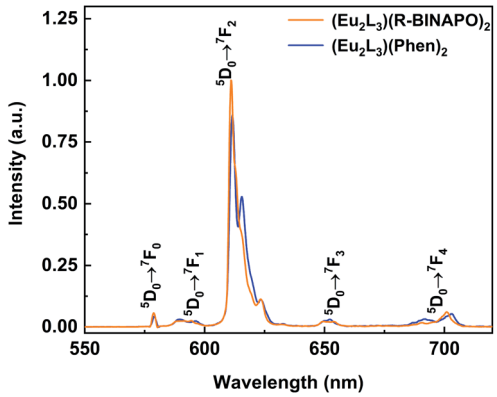

Fig. 4 Emission spectra of complexes $Eu_2L_3(Phen)_2$ and Eu_2L_3(*R*-BINAPO)$_2$ in THF (λ_{ex} = 370 nm, $c = 1.0 \times 10^{-5}$ M).

Another manner to infer the symmetry of Eu^{3+} site is to count the numbers of crystal-field splits.[21] On the basis of $^5D_0 \rightarrow {}^7F_2$ transitions with the five peaks at 612 nm (detailed splits can be seen from the deconvolution analyses in Fig. S13†), the local symmetry around Eu^{3+} ions in $Eu_2\mathbf{L}_3(Phen)_2$ and $Eu_2\mathbf{L}_3$(-BINAPO)$_2$ were most probably to be C_1. However, the assignment of the point group symmetry was not in line with that observed D_{4d} coordination geometry calculated from the single crystal structure of $Eu_2\mathbf{L}_3(Phen)_2$ (Fig. S10†). It is reasonable to consider the possibility of the presence of different coordination geometries around Eu^{3+} ion in solution and in solid state.[22]

The large ratio of $I(^5D_0 \rightarrow {}^7F_J)/I(^5D_0 \rightarrow {}^7F_1)$ transition generally implies that the complex has a relatively large radiative transition probability as judged from eqn (1).

$$k_r = \frac{1}{\tau_{rad}} = A_{MD,0} n^3 \left(\frac{I_{tot}}{I_{MD}}\right) \quad (1)$$

The radiative rate constant (k_r) is proportional to the intensity ratio of I_{tot}/I_{MD}, I_{tot} and I_{MD} represent the total integrated emission of $^5D_0 \rightarrow {}^7F_J$ and $^5D_0 \rightarrow {}^7F_1$ transitions, respectively. $A_{MD,0}$ is a constant (14.65 s^{-1}), representing the spontaneous emission probability of $^5D_0 \rightarrow {}^7F_1$ transition. n is the refractive index of solution.

The large k_r value does not indicate the high luminescence efficiency of Eu^{3+} center, because the non-radiative transition (k_{nr}) is inevitable. The both deactivation pathways finally determine the intrinsic quantum yields (Φ_{Eu}) as shown in eqn (2).

$$\Phi_{Ln} = \frac{k_r}{k_r + k_{nr}} = \frac{\tau_{obs}}{\tau_{rad}} \quad (2)$$

τ_{obs} is the experimental lifetimes. From the emission decay curves of Eu^{3+} ion monitored at the $^5D_0 \rightarrow {}^7F_2$ transition (Fig. S14 and S15†), the lifetimes of $Eu_2\mathbf{L}_3(Phen)_2$, $Eu_2\mathbf{L}_3$(*S*-BINAPO)$_2$ and $Eu_2\mathbf{L}_3$(*R*-BINAPO)$_2$ were fitted to be 613, 635 and 635 μs, respectively. On the basis of the calculated radiative lifetimes (τ_{rad}) and measured lifetimes, Φ_{Eu} were calculated to reach up to 74% and 84% for $Eu_2\mathbf{L}_3(Phen)_2$ and $Eu_2\mathbf{L}_3$(*R*/*S*-BINAPO)$_2$. With eqn (2), the radiative (k_r) and nonradiative rate constants (k_{nr}) were estimated and listed in Table 1. Additionally, the complexes also showed the large Eu^{3+} center luminescence quantum yields ($\Phi_{overall}$) of 31% and 34% for $Eu_2\mathbf{L}_3(Phen)_2$ and $Eu_2\mathbf{L}_3$(*R*/*S*-BINAPO)$_2$ (Fig. S16–S18†).

$$\Phi_{overall} = \eta_{sen}\Phi_{Ln} \quad (3)$$

From the eqn (3), the sensitizing efficiency (η_{sen}) was also calculated. In Eu^{3+} complexes, the energy level difference ΔE ($T_1 - {}^5D_0$) between the triplet states (T_1) of ligands and $^5D_0$ energy level of Eu^{3+} ion usually determined the sensitizing efficiency. An empirical energy gap to realize a highly effective energy transfer was proposed to be in range of 2500–5000 cm^{-1} for Eu^{3+} complexes.[23] By virtue of phosphorescence spectra of the Gd^{3+} complexes, the ΔE were estimated to be 3246 and 2540 cm^{-1} for $Eu_2\mathbf{L}_3(Phen)_2$ and $Eu_2\mathbf{L}_3$(*R*/*S*-BINAPO)$_2$ (Fig. S19†), which exactly located at the proposed energy gap range. In addition, the possible energy transfer from ancillary ligands to Eu^{3+} ion was excluded because of the absence of the excitation bands attributing to Phen and BINAPO.

Chiroptical properties of $Eu_2\mathbf{L}_3$(*R*/*S*-BINAPO)$_2$

In view of the introduction of chiral *R*-BINAPO and *S*-BINAPO and above spectral analyses, it was inferred that chiral ancillary could regulate the diastereoselective self-assembly of triple-stranded helicate. Therefore, the chirality of the helicate was firstly characterized by CD spectroscopy. From the Fig. 5, the two complexes $Eu_2\mathbf{L}_3$(*S*-BINAPO)$_2$ and $Eu_2\mathbf{L}_3$(*R*-BINAPO)$_2$ showed mirror-image Cotton effect in ranges of 250–400 nm, relating to the UV-vis absorption region of helicates. Moreover, two clear exciton couplings were observed in range of 250–315 and 315–400 nm, which were ascribed to the transitions from chiral BINAPO and achiral **L** ligand, respectively. In $Eu_2\mathbf{L}_3$(*R*-BINAPO)$_2$, a negative exciton coupling (a negative and positive signals at 300 and 260 nm) attributed to *R*-BINAPO was observed; conversely, a positive exciton coupling was obtained in case of *S*-BINAPO. Notably, the achiral **L** also present the chiroptical signal with a positive exciton coupling for $Eu_2\mathbf{L}_3$(*S*-BINAPO)$_2$ and a negative case for $Eu_2\mathbf{L}_3$(*R*-BINAPO)$_2$. It implied that the chirality was transferred from chiral phosphine oxide ancillary ligands to achiral **L** through the generation of supramolecular chirality.

The exciton coupling in metal complexes originated from the interactions of chromophores, in which the electron transition was no longer localized at one ligand, but became delocalization over the entire assemblies. Here, three bis-β-diketone were ligated at two metal centers, which forced them to close together. From the suggested empirical rule,[24] the relationships between the absolute configurations of the metal centers and the couplet signs have been built. Generally, the negative exciton couplet related to a Δ configuration of metal center; conversely, the positive exciton couplet correlated a Λ configuration. From this rule, the configurations estimated from the optimized molecular structures were in line with the observed CD patterns.

The excited state chiroptical property can be confirmed from the CPL spectra of helicates. As shown in Fig. 6, a pair of mirror-

Open Access Article. Published on 10 March 2021. Downloaded on 2/14/2026 12:17:19 PM. This article is licensed under a Creative Commons Attribution-NonCommercial 3.0 Unported Licence.

Table 1 Radiative (k_r) and nonradiative (k_{nr}) decay rate constants, measured emission lifetime of Eu^{3+} (τ_{obs}), sensitization efficiency (η_{sens}), intrinsic quantum yield (Φ_{Eu}), and overall quantum yield ($\Phi_{overall}$), g_{lum} values for $^5D_0 \rightarrow {}^7F_J$ of Eu^{3+} ion. Error in τ_{obs}: ±0.05 ms; 10% relative error in the other values; $\lambda_{ex} = 370$ nm

Complexes	k_r (s^{-1})	k_{nr} (s^{-1})	τ_{obs} (μs)	Φ_{Eu} (%)	η_{sens} (%)	$\Phi_{overall}$ (%)	g_{lum} $^5D_0 \rightarrow {}^7F_J$ ($J = 0, 1, 2, 3, 4$)				
							$J = 0$	$J = 1$	$J = 2$	$J = 3$	$J = 4$
Eu_2L_3(*R*-BINAPO)$_2$	1328	245	635	84	40	33.7	0.006	0.112	−0.009	0.003	−0.001
Eu_2L_3(*S*-BINAPO)$_2$	1327	247	635	84	41	34.3	−0.006	−0.112	0.009	−0.029	0.001
Eu_2L_3(Phen)$_2$	1208	422	613	74	42	30.8	—	—	—	—	—

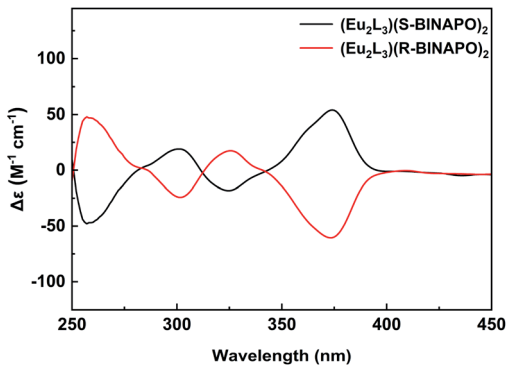

Fig. 5 CD spectra of Eu_2L_3(*S*-BINAPO)$_2$ (black line) and Eu_2L_3(*R*-BINAPO)$_2$ (red line) in THF (1.0×10^{-5} M).

image CPL signals appeared at the $^5D_0 \rightarrow {}^7F_J$ ($J = 0$–4) transition region. In these bands, the $^5D_0 \rightarrow {}^7F_2$ and $^5D_0 \rightarrow {}^7F_1$ transitions present the larger CPL intensities than other $^5D_0 \rightarrow {}^7F_{0,3,4}$ transition. The strong $^5D_0 \rightarrow {}^7F_2$ emission was due to the largest emitting intensity at 612 nm. In contrast, the $^5D_0 \rightarrow {}^7F_1$ transition at 595 nm also displayed a relatively large intensity, although its total emission was low. This mainly benefitted from its magnetic dipole transition characteristic. The luminescence dissymmetry factor, g_{lum} value ($-2 \leq g_{lum} \leq 2$) is the standard to estimate the excess of left *vs.* right circularly polarized luminescence, where $g_{lum} = 2(I_L - I_R)/(I_L + I_R)$, I_R and I_L refer to the left and right circularly polarized emission intensities, respectively. The $|g_{lum}|$ values of the $^5D_0 \rightarrow {}^7F_J$ transitions were summarized in Table 1. The largest $|g_{lum}|$ values were measured to be about 0.112 for $^5D_0 \rightarrow {}^7F_1$ transition at 595 nm, while the $^5D_0 \rightarrow {}^7F_2$ transitions were about 0.009. These results were comparable to the previously reported CPL Eu^{3+} complexes.[25]

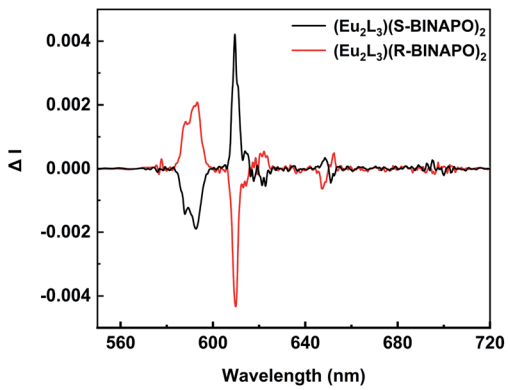

Fig. 6 CPL spectra of Eu_2L_3(*S*-BINAPO)$_2$ (black line) and Eu_2L_3(*R*-BINAPO)$_2$ (red line) ($\lambda_{ex} = 370$ nm, 1.0×10^{-5} M in THF).

Conclusions

In summary, we successfully synthesized an optical inactive helicate Eu_2L_3(Phen)$_2$ and a pair of optical active enantiomers Eu_2L_3(*S*-BINAPO)$_2$ and Eu_2L_3(*R*-BINAPO)$_2$ by employing achiral Phen and chiral *R*/*S*-BINAPO as second ligands. X-ray crystallographic analysis revealed that achiral ancillary could not control the stereoselective in the self-assembly process of the helicate, only a racemate could be obtained. Whereas, in the case of chiral BINAPO as ancillary ligands, the diastereoselectivity was realized. The mirror-image CD and CPL signs combining the NMR and semiempirical mechanical methodology proved that the chiral BINAPO could regulate the diastereoselective self-assembly of lanthanide helicate. In addition, the introduction of ancillary ligands not only offer the possibility for obtaining optical pure lanthanide helicate, but also increase the luminescence quantum yields from Eu^{3+} center and achieve a modest circularly polarized luminescence (CPL) with $|g_{lum}|$ values reaching to 0.112.

Experimental

Materials and instruments

Diphenyl sulfide, ethyl trifluoroacetate, 1,10-phenanthroline, (*R*/*S*)-BINAPO and $LnCl_3 \cdot 6H_2O$ salts (Ln = Eu and Gd) were purchased from Chembee Chemical Reagent Co., Ltd. (China); other chemicals and solvents are of analytical reagent grade.

The NMR experiments were measured on a Bruker Avance III 400 MHz spectrometer. EI-MS and ESI-TOF-MS were recorded on Agilent 5975N and Bruker maXis mass spectrometers, respectively.

Elemental analyses were recorded on an Elementar Vario EL cube analyzer. Single crystal X-ray crystal data of Ln_2L_3(Phen)$_2$ were recorded on a Xcalibur, Eos, Gemini diffractometer with Mo Kα radiation ($\lambda = 0.71073$ Å). The structure was solved by direct methods and refined on F^2 by full-matrix least-squares

© 2021 The Author(s). Published by the Royal Society of Chemistry

Open Access Article. Published on 10 March 2021. Downloaded on 2/14/2026 12:17:19 PM. This article is licensed under a Creative Commons Attribution-NonCommercial 3.0 Unported Licence.

using the SHELXTL-2018 program.[26] UV-vis spectra were measured by a PerkinElmer Lambda 25 spectrometer. Photoluminescence spectra containing the emission, excitation and luminescence lifetime measurements were recorded on an Edinburgh FLS 1000 spectrophotometer, and the luminescence quantum yield (Φ) were estimated by an integrating sphere equipped on this instrument. The Φ values were calculated using the following equation:

$$\Phi = \frac{\int L_{\text{emission}}}{\int E_{\text{reference}} - \int E_{\text{sample}}}$$

where $E_{\text{reference}}$ is the emission spectrum of the excitation light as only the reference in the sphere, E_{sample} is the emission spectrum of the excitation light as only the sample in the sphere, L_{emission} is the emission spectrum of the sample. The method is accurate within 10%. CD and CPL experiments were performed on an Olis DM245 spectrofluorimeter.

Synthetic procedures

4,4′-Diacetyldiphenyl sulphide. Anhydrous $AlCl_3$ (2.15 g, 16.1 mmol) was added to 30 mL dichloromethane in a 100 mL round bottom flask and stirred for 5 min. Then acetyl chloride (1.27 g, 16.1 mmol) in 15 mL of dichloromethane was slowly added dropwise. After cooling to 0 °C with ice-bath, diphenyl sulfide (1.00 g, 5.37 mmol) in 15 mL of dichloromethane was added. After stirring overnight, the reaction solution was poured into 150 mL ice-water, then hydrolyzed with 0.5 M HCl. The crude product was extracted with CH_2Cl_2 for two times, the organic layer was combined and dried with anhydrous Na_2SO_4, then evaporated to remove the solutions *in vacuo*. Recrystallization the crude product from ethanol led to the white flake crystals (1.24 g, 86%). ^{1}H NMR (400 MHz, $CDCl_3$) δ 7.94–7.86 (m, 4H), 7.44–7.37 (m, 4H), 2.58 (s, 6H). EI-MS m/z 271.35 $(M + H)^+$.

4,4′-Bis(4,4,4-trifluoro-1,3-dioxobutyl)diphenyl sulphide (L). **L** was prepared by the Claisen condensation of 4,4′-diacetyldiphenyl sulphide and ethyl trifluoroacetate in 1,2-dimethoxyethane (DME). To add freshly prepared sodium methoxide (0.80 g, 14.8 mmol) and ethyl trifluoroacetate (2.11 g, 14.8 mmol) into a Schlenk bottle containing 30 mL DME, and stirred the solution to become clear and transparent. Then 4,4′-diacetyl phenyl sulfide (1.00 g, 3.7 mmol) was added, and then solution was stirred for 24 hours at room temperature. The final reaction solution was quenched with ice-water, then acidified to pH 2–3 using 2.0 M HCl solution, the resulting yellow precipitate was filtered and recrystallized from ethyl acetate solvents to give yellow flake crystal (1.26 g, 87%). ^{1}H NMR (400 MHz, THF-d_8): 8.09–8.07 (m, 4H), 7.55–753 (m, 4H), 6.83 (s, 2H). ESI-MS m/z 549.07 $[\mathbf{L} + (CH_3OH)_2 + Na]^+$.

Synthesis of $Ln_2L_3(Phen)_2$

L (1.00 g, 2.10 mmol), NEt_3 (0.70 g, 7.2 mmol) and 1,10-phenanthroline (0.50 g, 2.8 mmol) were dissolved in 30 mL methanol and stirred for 5 min, then $LnCl_3 \cdot 6H_2O$ (1.4 mmol) in 5 mL methanol was added, which was accompanied by the presence of a large amount of precipitation. The mixture was then refluxed for 12 h. After cooling to room temperature, the precipitation was filtered and washed by 10 mL CH_3OH and 10 mL H_2O, respectively, then dried under vacuum.

$Eu_2(L)_3(Phen)_2$. Yield: 72%. Anal. Calc. for $C_{84}H_{46}F_{18}N_4O_{12}S_3Eu_2$ (2045.4026): C, 49.33; H, 2.27; N, 2.74; S, 4.70. Found: C, 49.41; H, 2.49; N, 2.71; S, 4.82. ESI-MS: m/z = 2046.0363.

$Gd_2(L)_3(Phen)_2$. Yield: 82%. Anal. Calc. for $C_{84}H_{46}F_{18}N_4O_{12}S_3Gd_2$ (2055.9777): C, 49.33; H, 2.27; N, 2.74; S, 4.70. Found: C, 49.41; H, 2.29; N, 2.71; S, 4.82. ESI-MS: m/z = 2056.0778.

Synthesis of $Ln_2(L)_3$ ((*R*/*S*)-BINAPO)$_2$

L (1.00 g, 2.10 mmol), NEt_3 (0.70 g, 7.2 mmol) and (*R*/*S*)-BINAPO (1.9 g, 2.8 mmol) were dissolved in 30 mL methanol and stirred for 5 min, then $LnCl_3 \cdot 6H_2O$ (1.4 mmol) in 5 mL methanol was added, which was accompanied by the presence of a large amount of precipitation. The mixture was then refluxed for 12 h. After cooling to room temperature, the precipitation was filtered and washed by 10 mL CH_3OH and 10 mL H_2O, respectively, then dried under vacuum.

Eu_2L_3(*R*-BINAPO)$_2$. Yield: 81%. Anal. Calc. for $C_{148}H_{94}F_{18}O_{16}S_3P_4Eu_2$ (2994.34): C, 59.37; H, 3.16; S, 3.21. Found: C, 59.14; H, 3.21; S, 3.47. ^{1}H NMR (400 MHz, THF-d_8) δ 9.49 (s, 8H), 9.43–9.41 (m, 4H), 8.31–8.27 (m, 12H), 8.02–7.85 (m, 24H), 7.74–7.65 (m, 8H), 7.58–7.52 (m, 4H), 7.38–7.29 (m, 12H), 7.03–6.96 (m, 4H), 6.61–6.59 (m, 12H), 5.34 (s, 6H). ESI-MS: m/z = 2995.1156 $[M + H]^+$; 3017.1649 $[M + Na]^+$; 3033.1338 $[M + K]^+$.

Eu_2L_3(*S*-BINAPO)$_2$. Yield: 82%. Anal. Calc. for $C_{148}H_{94}F_{18}O_{16}S_3P_4Eu_2$ (2994.34): C, 59.37; H, 3.16; S, 3.21. Found: C, 59.26; H, 3.33; S, 3.09. ^{1}H NMR (400 MHz, THF-d_8) δ 9.49 (s, 8H), 9.43–9.41 (m, 4H), 8.31–8.27 (m, 12H), 8.02–7.85 (m, 24H), 7.74–7.65 (m, 8H), 7.58–7.52 (m, 4H), 7.38–7.29 (m, 12H), 7.03–6.96 (m, 4H), 6.61–6.59 (m, 12H), 5.34 (s, 6H). ESI-MS: m/z = 2995.1158 $[M + H]^+$; 3017.1653 $[M + Na]^+$; 3033.1340 $[M + K]^+$.

Gd_2L_3(*R*-BINAPO)$_2$. Yield: 84%. Anal. Calc. for $C_{148}H_{94}F_{18}O_{16}S_3P_4Gd_2$ (3004.28): C, 59.16; H, 3.15; S, 3.20. Found: C, 59.14; H, 3.19; S, 3.22. ESI-MS: m/z = 3005.9389 $[M + H]^+$.

Conflicts of interest

There are no conflicts to declare.

Acknowledgements

This work is financially supported by the National Natural Science Foundation of China (No. 520730805 & 51872077 & 51773054) for supporting this work.

References

1 (*a*) L. Zhang, H. Wang, S. Li and M. Liu, *Chem. Soc. Rev.*, 2020, **49**, 9095–9120; (*b*) M. Hu, H.-T. Feng, Y.-S. Yuan, Y.-S. Zheng and B.-Z. Tang, *Coord. Chem. Rev.*, 2020, **416**, 213329–213363; (*c*) W. Ma, L. Xu, A. F. de Moura, X. Wu, H. Kuang, C. Xu and N. A. Kotov, *Chem. Rev.*, 2017, **117**, 8041–8093; (*d*) Y. Sang, J. Han, T. Zhao, P. Duan and M. Liu, *Adv. Mater.*, 2020, **32**, 1900110–1900143; (*e*) W. Shang, X. Zhu, T. Liang, C. Du, L. Hu, T. Li and M. Liu,

Open Access Article. Published on 10 March 2021. Downloaded on 2/14/2026 12:17:19 PM. This article is licensed under a Creative Commons Attribution-NonCommercial 3.0 Unported Licence.

Angew. Chem., Int. Ed., 2020, **59**, 12811–12816; (*f*) L. Wang, L. Yin, W. Zhang, X. Zhu and M. Fujiki, *J. Am. Chem. Soc.*, 2017, **139**, 13218–13226.

2 (*a*) S. Huo, P. Duan, T. Jiao, Q. Peng and M. Liu, *Angew. Chem., Int. Ed.*, 2017, **56**, 12174–12178; (*b*) D.-Y. Kim, *J. Korean Phys. Soc.*, 2006, **49**, S505–S508; (*c*) F. Zinna, U. Giovanella and L. Di Bari, *Adv. Mater.*, 2015, **27**, 1791–1795; (*d*) E. J. Werner, A. Datta, C. J. Jocher and K. N. Raymond, *Angew. Chem., Int. Ed.*, 2008, **47**, 8568–8580; (*e*) T. W. Victor, K. H. O'Toole, L. M. Easthon, M. Ge, R. J. Smith, X. Huang, H. Yan, Y. S. Chu, S. Chen, D. Gursoy, M. Ralle, B. Imperiali, K. N. Allen and L. M. Miller, *J. Am. Chem. Soc.*, 2020, **142**, 2145–2149.

3 N. P. M. Huck, W. F. Jager, B. de Lange and B. L. Feringa, *Science*, 1996, **273**, 1686–1688.

4 (*a*) F. Zinna, S. Voci, L. Arrico, E. Brun, A. Homberg, L. Bouffier, T. Funaioli, J. Lacour, N. Sojic and L. Di Bari, *Angew. Chem., Int. Ed.*, 2019, **58**, 6952–6956; (*b*) M. Li, S.-H. Li, D. Zhang, M. Cai, L. Duan, M.-K. Fung and C.-F. Chen, *Angew. Chem., Int. Ed.*, 2018, **57**, 2889–2893; (*c*) J. F. Sherson, H. Krauter, R. K. Olsson, B. Julsgaard, K. Hammerer, I. Cirac and E. S. Polzik, *Nature*, 2006, **443**, 557–560.

5 (*a*) R. Sethy, J. Kumar, R. Métivier, M. Louis, K. Nakatani, N. M. T. Mecheri, A. Subhakumari, K. G. Thomas, T. Kawai and T. Nakashima, *Angew. Chem., Int. Ed.*, 2017, **56**, 15053–15057; (*b*) Y. Yang, R. C. da Costa, M. J. Fuchter and A. J. Campbell, *Nat. Photonics*, 2013, **7**, 634–638; (*c*) Y. Imai, Y. Nakano, T. Kawai and J. Yuasa, *Angew. Chem., Int. Ed.*, 2018, **57**, 8973–8978; (*d*) S. Shuvaev, E. A. Suturina, K. Mason and D. Parker, *Chem. Sci.*, 2018, **9**, 2996–3003; (*e*) K. Staszak, K. Wieszczycka, V. Marturano and B. Tylkowski, *Coord. Chem. Rev.*, 2019, **397**, 76–90; (*f*) M. Iwamura, M. Fujii, A. Yamada, H. Koike and K. Nozaki, *Chem.–Asian J.*, 2019, **14**, 561–567; (*g*) T. Wu, P. Bouř and V. Andrushchenko, *Sci. Rep.*, 2019, **9**, 1068–1073.

6 (*a*) S. V. Eliseeva and J.-C. G. Bünzli, *Chem. Soc. Rev.*, 2010, **39**, 189–227; (*b*) J. C. Bünzli and C. Piguet, *Chem. Soc. Rev.*, 2005, **34**, 1048–1077; (*c*) M. W. Loble, J. M. Keith, A. B. Altman, S. C. Stieber, E. R. Batista, K. S. Boland, S. D. Conradson, D. L. Clark, J. Lezama Pacheco, S. A. Kozimor, R. L. Martin, S. G. Minasian, A. C. Olson, B. L. Scott, D. K. Shuh, T. Tyliszczak, M. P. Wilkerson and R. A. Zehnder, *J. Am. Chem. Soc.*, 2015, **137**, 2506–2523; (*d*) E. G. Moore, A. P. S. Samuel and K. N. Raymond, *Acc. Chem. Res.*, 2009, **42**, 542–552.

7 (*a*) S. Feuillastre, M. Pauton, L. Gao, A. Desmarchelier, A. J. Riives, D. Prim, D. Tondelier, B. Geffroy, G. Muller, G. Clavier and G. Pieters, *J. Am. Chem. Soc.*, 2016, **138**, 3990–3993; (*b*) C. M. Cruz, S. Castro-Fernández, E. Maçôas, J. M. Cuerva and A. G. Campaña, *Angew. Chem., Int. Ed.*, 2018, **57**, 14782–14786; (*c*) P. Reiné, J. Justicia, S. P. Morcillo, S. Abbate, B. Vaz, M. Ribagorda, Á. Orte, L. Álvarez de Cienfuegos, G. Longhi, A. G. Campaña, D. Miguel and J. M. Cuerva, *J. Org. Chem.*, 2018, **83**, 4455–4463; (*d*) E. M. Sánchez-Carnerero, F. Moreno, B. L. Maroto, A. R. Agarrabeitia, M. J. Ortiz, B. G. Vo, G. Muller and S. de la Moya, *J. Am. Chem. Soc.*, 2014, **136**, 3346–3349; (*e*) M. Deng, N. D. Schley and G. Ung, *Chem. Commun.*, 2020, **56**, 14813–14816.

8 (*a*) D. E. Barry, J. A. Kitchen, L. Mercs, R. D. Peacock, M. Albrecht and T. Gunnlaugsson, *Dalton Trans.*, 2019, **48**, 11317–11325; (*b*) Y. Hasegawa, Y. Miura, Y. Kitagawa, S. Wada, T. Nakanishi, K. Fushimi, T. Seki, H. Ito, T. Iwasa, T. Taketsugu, M. Gon, K. Tanaka, Y. Chujo, S. Hattori, M. Karasawa and K. Ishii, *Chem. Commun.*, 2018, **54**, 10695–10697; (*c*) J. Zhang, L. Dai, A. M. Webster, W. T. K. Chan, L. E. Mackenzie, R. Pal, S. L. Cobb and G.-L. Law, *Angew. Chem., Int. Ed.*, 2021, **60**, 1004–1010; (*d*) V. Y. Chang, K. U. D. Calvinho, R. C. Tovar, V. A. Johnson, D. A. Straus and G. Muller, *Eur. J. Inorg. Chem.*, 2020, **2020**, 3815–3828; (*e*) J. G. Ski, P. Starynowicz, K. T. Hua, J. L. Lunkley, G. Muller and J. Lisowski, *J. Am. Chem. Soc.*, 2008, **130**, 17761–17773.

9 (*a*) Z. Shen, Y. Sang, T. Wang, J. Jiang, Y. Meng, Y. Jiang, K. Okuro, T. Aida and M. Liu, *Nat. Commun.*, 2019, **10**, 3976–3983; (*b*) Z.-B. Sun, J.-K. Liu, D.-F. Yuan, Z.-H. Zhao, X.-Z. Zhu, D.-H. Liu, Q. Peng and C.-H. Zhao, *Angew. Chem., Int. Ed.*, 2019, **58**, 4840–4846; (*c*) S. Lee, K. Y. Kim, S. H. Jung, J. H. Lee, M. Yamada, R. Sethy, T. Kawai and J. H. Jung, *Angew. Chem., Int. Ed.*, 2019, **58**, 18878–18882; (*d*) K. Takaishi, M. Yasui and T. Ema, *J. Am. Chem. Soc.*, 2018, **140**, 5334–5338; (*e*) K. Takaishi, K. Iwachido and T. Ema, *J. Am. Chem. Soc.*, 2020, **142**, 1774–1779; (*f*) Y. Li, A. Yagi and K. Itami, *J. Am. Chem. Soc.*, 2020, **142**, 3246–3253.

10 J. L. Lunkley, D. Shirotani, K. Yamanari, S. Kaizaki and G. Muller, *J. Am. Chem. Soc.*, 2008, **130**, 13814–13815.

11 F. Stomeo, C. Lincheneau, J. P. Leonard, J. E. O'Brien, R. D. Peacock, C. P. McCoy and T. Gunnlaugsson, *J. Am. Chem. Soc.*, 2009, **131**, 9636–9637.

12 (*a*) O. Kotova, S. Comby, K. Pandurangan, F. Stomeo, J. E. O'Brien, M. Feeney, R. D. Peacock, C. P. McCoy and T. Gunnlaugsson, *Dalton Trans.*, 2018, **47**, 12308–12317; (*b*) D. E. Barry, J. A. Kitchen, K. Pandurangan, A. J. Savyasachi, R. D. Peacock and T. Gunnlaugsson, *Inorg. Chem.*, 2020, **59**, 2646–2650; (*c*) S. J. Bradberry, G. Dee, O. Kotova, C. P. McCoy and T. Gunnlaugsson, *Chem. Commun.*, 2019, **55**, 1754–1757; (*d*) J. A. Thomas, *Dalton Trans.*, 2011, **40**, 12005–12016.

13 (*a*) X.-Z. Li, L.-P. Zhou, L.-L. Yan, D.-Q. Yuan, C.-S. Lin and Q.-F. Sun, *J. Am. Chem. Soc.*, 2017, **139**, 8237–8244; (*b*) L.-X. Cai, L.-L. Yan, S.-C. Li, L.-P. Zhou and Q.-F. Sun, *Dalton Trans.*, 2018, **47**, 14204–14210; (*c*) Q.-Y. Zhu, L.-P. Zhou, L.-X. Cai, X.-Z. Li, J. Zhou and Q.-F. Sun, *Chem. Commun.*, 2020, **56**, 2861–2864.

14 C. T. Yeung, W. T. Chan, S. C. Yan, K. L. Yu, K. H. Yim, W. T. Wong and G.-L. Law, *Chem. Commun.*, 2015, **51**, 592–595.

15 (*a*) Y. B. Tan, M. Yamada, S. Katao, Y. Nishikawa, F. Asanoma, J. Yuasa and T. Kawai, *Inorg. Chem.*, 2020, **59**, 12867–12875; (*b*) Y. Kitagawa, M. Tsurui and Y. Hasegawa, *ACS Omega*, 2020, **5**, 3786–3791; (*c*) C. Dee, F. Zinna, E. Kreidt, L. Arrico, A. Rodríguez-Rodríguez, C. Platas-Iglesias, L. Di Bari and M. Seitz, *J. Rare Earths*, 2020, **38**,

© 2021 The Author(s). Published by the Royal Society of Chemistry

Open Access Article. Published on 10 March 2021. Downloaded on 2/14/2026 12:17:19 PM.
This article is licensed under a Creative Commons Attribution-NonCommercial 3.0 Unported Licence.

564–570; (*d*) L. Arrico, C. De Rosa, L. Di Bari, A. Melchior and F. Piccinelli, *Inorg. Chem.*, 2020, **59**, 5050–5062; (*e*) F. Zinna, L. Arrico and L. Di Bari, *Chem. Commun.*, 2019, **55**, 6607–6609; (*f*) M. Starck, L. E. MacKenzie, A. S. Batsanov, D. Parker and R. Pal, *Chem. Commun.*, 2019, **55**, 14115–14118; (*g*) Y. B. Tan, Y. Okayasu, S. Katao, Y. Nishikawa, F. Asanoma, M. Yamada, J. Yuasa and T. Kawai, *J. Am. Chem. Soc.*, 2020, **142**, 17653–17661; (*h*) T. Y. Bing, T. Kawai and J. Yuasa, *J. Am. Chem. Soc.*, 2018, **140**, 3683–3689.

16 (*a*) Y. Zhang, Y. Zhou, T. Gao, P. Yan and H. Li, *Chem. Commun.*, 2020, **56**, 13213–13216; (*b*) Z. Zhang, Y. Zhou, H. Li, T. Gao and P. Yan, *Dalton Trans.*, 2019, **48**, 4026–4034.

17 (*a*) Y. Zhou, H. Li, T. Zhu, T. Gao and P. Yan, *J. Am. Chem. Soc.*, 2019, **141**, 19634–19643; (*b*) G. Han, Y. Zhou, Y. Yao, Z. Cheng, T. Gao, H. Li and P. Yan, *Dalton Trans.*, 2020, **49**, 3312–3320; (*c*) Y. Zhou, Y. Yao, Z. Cheng, T. Gao, H. Li and P. Yan, *Inorg. Chem.*, 2020, **59**, 12850–12857; (*d*) M. Dubey, A. Kumar, V. M. Dhavale, S. Kurungot and D. S. Pandey, *CrystEngComm*, 2015, **17**, 8202–8206; (*e*) S. Bi, Y. Zhou, Y. Yao, Z. Cheng, T. Gao, P. Yan and H. Li, *Aust. J. Chem.*, 2020, **74**, 145–150.

18 (*a*) D. Liu, Y. Zhou, Y. Zhang, H. Li, P. Chen, W. Sun, T. Gao and P. Yan, *Inorg. Chem.*, 2018, **57**, 8332–8337; (*b*) K. T. Hua, J. Xu, E. E. Quiroz, S. Lopez, A. J. Ingram, V. A. Johnson, A. R. Tisch, A. de Bettencourt-Dias, D. A. Straus and G. Muller, *Inorg. Chem.*, 2012, **51**, 647–660; (*c*) M. Leonzio, M. Bettinelli, L. Arrico, M. Monari, L. Di Bari and F. Piccinelli, *Inorg. Chem.*, 2018, **57**, 10257–10264; (*d*) M. Gorecki, L. Carpita, L. Arrico, F. Zinna and L. Di Bari, *Dalton Trans.*, 2018, **47**, 7166–7177; (*e*) J. Yuasa, H. Ueno and T. Kawai, *Chem*, 2014, **20**, 8621–8627; (*f*) T. Harada, Y. Nakano, M. Fujiki, M. Naito, T. Kawai and Y. Hasegawa, *Inorg. Chem.*, 2009, **48**, 11242–11250.

19 J. D. L. Dutra, T. D. Bispo and R. O. Freire, *J. Comput. Chem.*, 2014, **35**, 772–775.

20 T. Zhu, P. Chen, H. Li, W. Sun, T. Gao and P. Yan, *Phys. Chem. Chem. Phys.*, 2015, **17**, 16136–16144.

21 C. Görller-Walrand and K. Binnemans, *Handbook on the Physics and Chemistry of Rare Earths*, Elsevier, Amsterdam, 1996, pp. 121–283.

22 D. Shirotani, T. Suzuki and S. Kaizaki, *Inorg. Chem.*, 2006, **45**, 6111–6113.

23 (*a*) F. J. Steemers, W. Verboom, D. N. Reinhoudt, E. B. van der Tol and J. W. Verhoeven, *J. Am. Chem. Soc.*, 1995, **117**, 9408–9414; (*b*) M. Latva, H. Takalo, V.-M. Mukkala, C. Matachescu, J. C. Rodriguez-Ubis and J. Kankare, *J. Lumin.*, 1997, **75**, 149–169.

24 (*a*) S. D. Bonsall, M. Houcheime, D. A. Straus and G. Muller, *Chem. Commun.*, 2007, **35**, 3676–3678; (*b*) S. Petoud, G. Muller, E. G. Moore, J. Xu, J. Sokolnicki, J. P. Riehl, U. N. Le, S. M. Cohen and K. N. Raymond, *J. Am. Chem. Soc.*, 2007, **129**, 77–83.

25 (*a*) M. Seitz, K. Do, A. J. Ingram, E. G. Moore, G. Muller and K. N. Raymond, *Inorg. Chem.*, 2009, **48**, 8469–8479; (*b*) K. Okutani, K. Nozaki and M. Iwamura, *Inorg. Chem.*, 2014, **53**, 5527–5537; (*c*) M. Leonzio, A. Melchior, G. Faura, M. Tolazzi, F. Zinna, L. Di Bari and F. Piccinelli, *Inorg. Chem.*, 2017, **56**, 4413–4421; (*d*) O. Kotova, S. Blasco, B. Twamley, J. O'Brien, R. D. Peacock, J. A. Kitchen, M. Martínez-Calvo and T. Gunnlaugsson, *Chem. Sci.*, 2015, **6**, 457–471; (*e*) C.-T. Yeung, K.-H. Yim, H.-Y. Wong, R. Pal, W.-S. Lo, S.-C. Yan, M. Yee-Man Wong, D. Yufit, D. E. Smiles, L. J. McCormick, S. J. Teat, D. K. Shuh, W.-T. Wong and G.-L. Law, *Nat. Commun.*, 2017, **8**, 1128–1137; (*f*) N. Shi, R. Wang, X. Wang, J. Tan, Y. Guan, Z. Li, X. Wan and J. Zhang, *Chem. Commun.*, 2019, **55**, 1136–1139.

26 G. M. Sheldrick, *Acta Crystallogr., Sect. C: Struct. Chem.*, 2015, **71**, 3–8.

© 2021 The Author(s). Published by the Royal Society of Chemistry